A comparative numerical study of premixed and non-premixed ethylene flames

FOKION N. EGOLFOPOULOS[a] and PAUL E. DIMOTAKIS[b]

[a]*Aerospace & Mechanical Engineering Department, University of Southern California, Los Angeles, CA 90089-1453 and* [b]*Graduate Aeronautical Laboratories, California Institute of Technology, Pasadena, CA 91125.*

Detailed numerical simulations of premixed and non-premixed C_2H_4/air flames were conducted, using six available kinetic mechanisms. The results help assess differences between these mechanisms and are of interest to proposed hydrocarbon-fueled SCRAMJET concepts, in which C_2H_4 can be expected to be a major component of the thermally cracked fuel. For premixed flames, laminar flame speeds were calculated and compared with available experimental data. For non-premixed flames, ignition/extinction Z-curves were calculated for conditions of relevance to proposed SCRAMJET concepts. Results revealed a large variance in predictions of the kinetic mechanisms examined. Differences in laminar flame speeds as high as factors of 2.5 were found. For the conditions investigated, computed ignition and extinction strain rates for non-premixed flames differed by factors as high as 300 and 3, respectively. This indicates that while there are differences in high-temperature kinetics that control flame propagation and extinction, discrepancies in low-temperature kinetics that control ignition can be even more significant. Sensitivity- and species-consumption analyses indicate uncertainties in fuel kinetics and, most importantly, on the oxidation of C_2H_3 and the production of CH_2CHO, whose kinetics are not well known and can crucially affect production of the important H radicals. These findings stress the need for experimental data in premixed and non-premixed configurations that can be used to assess these phenomena and provide the basis for a comprehensive validation.

1. INTRODUCTION

Ethylene (C_2H_4) is an intermediate in the oxidative sequence of high-C hydrocarbons (*e.g.*, Westbrook & Dryer 1981, Bhargava & Westmoreland 1998a,b). However, C_2H_4 kinetics are not well understood, compared to the extensively studied methane (CH_4) kinetics, for example. Furthermore, there are challenges in describing the kinetics of the destruction paths of the vinyl radical (C_2H_3) (*e.g.*, Marinov *et al*. 1995; Bhargava & Westmoreland

1998a,b; Marinov 1998; Wang *et al*. 1999). C_2H_3 is the major product of hydrogen abstraction from C_2H_4. Any uncertainties at this level of oxidation can compromise the fidelity of the overall mechanism in predicting flame properties.

The use of C_2H_4 as a practical fuel is also relevant to high-Mach-number, air-breathing propulsion concepts (*e.g.*, Edwards 1996). The concepts pertain to flight Mach numbers, M_∞, in the range $4 < M_\infty < 8$, and rely on the use of endothermic high-C hydrocarbon fuels that can be used as coolants for the fuselage and internal-flow passages. As a result, the hydrocarbon fuel will be heated to temperatures that result in thermal cracking of the parent fuel molecule. Cracking yields a fuel mix of lower-C hydrocarbons, eventually fed to the SCRAMJET combustor. Fuel temperatures as high as 800 K to 1050 K are expected (Edwards 1996). Assuming $C_{12}H_{26}$ to be the main constituent of kerosene-type fuels, the resulting fuel mix, under such conditions, is primarily composed of approximately equal amounts of CH_4 and C_2H_4 (Egolfopoulos & Dimotakis 1998, 2000). Thus, the description of SCRAMJET combustion becomes particularly sensitive to the details of C_2H_4 kinetics; C_2H_4 in this case is the supplied fuel and not only an intermediate.

The accurate description of the combustion response of proposed SCRAMJET concepts, is more important compared to conventional low-speed applications, with hydrodynamic time scales that are very small (high strain rates). A good description of ignition and extinction processes is essential to design. Previous numerical studies (Egolfopoulos & Dimotakis 1998) focused on the ignition/extinction characteristics of fuel mixes expected from thermal cracking. The presence of CH_4 inhibited the ignition characteristics of C_2H_4. Minor changes in C_2H_3 kinetics were found capable of modifying predicted ignition strain rates of pure C_2H_4 by factors as high as 30. A subsequent numerical study (Egolfopoulos & Dimotakis 2000) focused on the ignition/extinction response of pure C_2H_4 and its potential ignition-enhancement through independent and simultaneous additions of such additives as NO and F_2. While these promote ignition, the overall response was found to be rather sensitive to C_2H_4 oxidation kinetics.

The main goal of the present work is the comparison of predictions of a number of available mechanisms on C_2H_4 kinetics in flames. The results will help assess the state of current knowledge on the subject and the relative ability of these mechanisms to predict fundamental flame properties.

2. APPROACH

Freely propagating, one-dimensional, premixed flames and opposed-jet, stagnation-flow, non-premixed flame configurations were chosen for the study, the latter to quantify the effect of fluid mechanics on ignition and extinction of non-premixed flames. Freely propagating flames were simulated to determine laminar flame speeds, S_u^o, for which reliable experimental data are available. Their prediction is a validation requirement for any mechanism. Flame propagation is very sensitive to various elementary reactions, especially those of the H_2/CO subsystem. At the same time, the rate of evolution of H_2/CO kinetics depends on a number of oxidation reactions of the parent fuel molecule (*e.g.*, Westbrook & Dryer 1981, Marinov *et al*. 1995, Marinov 1998), which, in many cases, can be "bottlenecks" of the overall burning process.

Laminar flame speeds were calculated using the PREMIX Sandia code (Kee *et al*. 1985) modified to allow for thermal radiation from CO, CO_2, and H_2O (Law & Egolfopoulos 1992). The opposed-jet configuration was simulated by solving the conservation equations of mass, momentum, energy, and species concentrations along the stagnation streamline (Egolfopoulos 1994, Egolfopoulos & Campbell 1996) for steady flow. The opposed-jet code employed a two-point continuation approach to describe the entire Z-curve flame response to strain rate variation (Nishioka *et al*. 1996; Egolfopoulos & Dimotakis 1998, 2000). The codes were integrated with the CHEMKIN (Kee *et al*. 1989) and Transport (Kee *et al*. 1983) subroutine libraries.

3. CHEMICAL KINETICS MECHANISMS

Six, recently compiled, kinetic mechanisms were chosen. All mechanisms were tested including the thermodynamic and transport data set used for each compilation. These are:

1. The Tan *et al*. (1994) mechanism, hereafter referred to as "TAN94", is a comprehensive mechanism developed to describe the oxidation of CH_4, C_2H_4, C_2H_2, propane (C_3H_8), and propene (C_3H_6), individually and also as blends. The mechanism relies on 78 species and 473 reactions.

2. The GRI 2.1 mechanism (Frenklach *et al*. 1995) hereafter referred to as "GRI21", was originally developed to describe a number of flame properties of methane/air mixtures, as well as methane oxidation in homogeneous systems. It contains kinetics of $H_2/CO/C_1/C_2$ species and has been widely used the last 4-5 years in simulations of C_1- and C_2- hydrocarbon flames. GRI21 also contains a C_2H_4 kinetics subset and is a mechanism compiled hierarchically and as such the H_2/CO and CH_4 subsets can be used with confidence. The mechanism relies on 31 species and 175 reactions.

3. The Wang & Frenklach (1997) mechanism, hereafter referred to as "WF97", was developed for the description of the formation and growth of polycyclic aromatic hydrocarbons. It maintains the basic features of GRI21, and, similarly to GRI30, it was augmented through the addition of a few species to better describe C_2H_4 and acetylene (C_2H_2) flames. The mechanism relies on 33 species and 192 reactions.

4. The Marinov *et al*. (1998) mechanism, hereafter referred to as "MRN98", was developed through tests against C_2H_4, C_2H_2, and ethanol (C_2H_5OH) flames. The mechanism relies on 57 species and 383 reactions. An earlier version of its C_2H_4/C_2H_2 kinetic subsets (Marinov *et al*. 1995), relying on 46 species and 246 reactions was tested against experimental laminar flame speeds for C_2H_4/air and C_2H_2/air flames (Egolfopoulos *et al*. 1990).

5. The GRI 3.0 mechanism (Bowman *et al*. 1999), hereafter referred to as "GRI30", was recently released and retains the basic features of GRI21. It was augmented through additional species relevant to C_2H_4, the most important of which was vinyoxy (CH_2CHO). A limited number of C_3-related kinetic steps were also added. The mechanism relies on 35 species and 217 reactions.

6. The Wang *et al*. (1999) mechanism, hereafter referred to as "W99", was recently developed to describe the combustion characteristics of C_2H_4, C_2H_2, and C_3H_x fuels. In this model, small-species chemistry is largely based on GRI 2.1 mechanism (Frenklach *et al*. 1995). The reaction kinetics of acetylene and ethylene are based work reported previously (Sun *et al*. 1996, Wang & Frenklach 1997, Laskin & Wang 1999). The C_3H_x sub-model was taken from (Davis *et al*. 1999). The kinetic model retains a reasonable number of C_4 species to ensure proper simulation under fuel-rich conditions. The mechanism relies on 52 species and 367 reactions.

4. RESULTS AND DISCUSSION

4.1 Reactant inflow conditions

Laminar flame speeds were calculated for atmospheric C_2H_4/air mixtures for a wide range of equivalence ratio, ϕ, and for an unburned mixture temperature, T_{unb} = 300 K, for which experimental data are available (Egolfopoulos *et al*. 1990).

Ignition/extinction Z-curves for non-premixed, opposed-jet configurations were determined by impinging an air stream on a counterflowing C_2H_4 stream, at p = 1 atm. The simulations were conducted for a fuel-stream temperature T_{fuel} = 950 K, and for an air-stream temperature T_{air} = 1200 K. While the choice of T_{fuel} is consistent with one used in previous studies (Egolfopoulos & Dimotakis 1998, 2000), an air temperature of T_{air} = 1200 K was chosen as the minimum air temperature for which all mechanisms produce ignition. Z-curves were calculated initializing with vigorously burning flames and gradually reducing the H-radical pool, following the two-point continuation approach described above. They were represented through the variation of the maximum mass fraction of H radicals, Y_{Hmax}, with strain rate, σ. The latter was defined as minus the convective velocity gradient, on the air side, just before the main chemical-activity zone. Through sensitivity analyses (Kee *et al*. 1985) and integrated species-consumption path analyses (Egolfopoulos & Dimotakis 1998, 2000), the details controlling flame propagation as well as the Z-curve ignition/extinction response were identified.

4.2 Laminar flame speeds

Figure 1 depicts the experimental and calculated values of S_u^o. Discrepancies in the predictions of S_u^o are evident. For stoichiometric (ϕ = 1.0) and rich (ϕ = 1.6) flames, for example, S_u^o predictions vary by as much as a factor of 1.6 and 2.5 respectively, a range considered excessive for flame propagation. Adjusting for agreement would require significant modification in the kinetics.

GRI30 produces the highest values, while MRN98 the lowest. TAN94 and W99 achieve best agreement with experimental values. The low predictions of MRN98 are not in accord with previously reported comparisons (Marinov *et al*. 1995). Some discrepancies pertaining to the

C_2H_4 kinetic subset may exist between the two mechanisms (the Marinov *et al.* 1995 mechanism was not available to us).
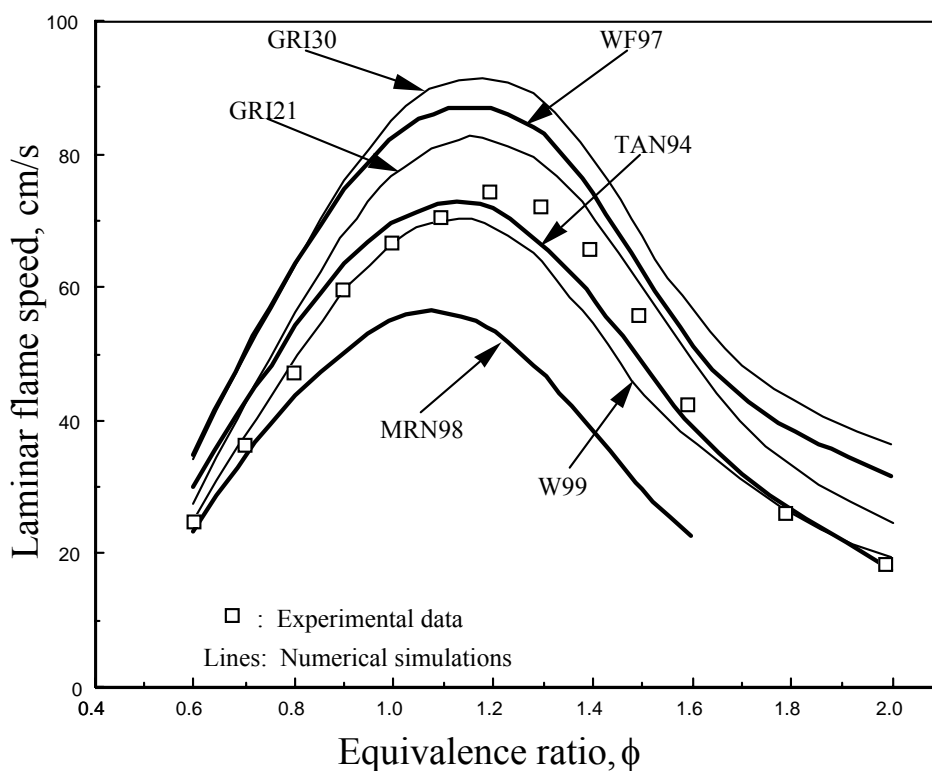

FIGURE 1.   Calculated laminar flame speeds for atmospheric C_2H_4/air flames with $T_{unb} = 300$ K and comparison with experimental data (Egolfopoulos *et al.* 1990).

Figures 2 and 3 depict the effect of the various mechanisms on the normalized sensitivity coefficients (SC) on the mass-burning rate of a stoichiometric ($\phi = 1.0$) C_2H_4/air flame. Given the large number of reactions involved, only those characterized by the greatest sensitivity are presented.

All mechanisms examined yield similar, positive SC's for the $H+O_2 \rightarrow OH+O$ and $CO+OH \rightarrow CO_2+H$ reactions, that are chiefly responsible for radical branching and heat release, respectively. All mechanisms also have similar, positive SC's for the H-producing $HCO+M \rightarrow CO+H+M$ reaction. Noticeable SC's to C_2H_4 H-abstraction reactions are observed for WF97, GRI30, and W99 ($C_2H_4+OH \rightarrow C_2H_3+H_2O$) and TAN94 ($C_2H_4+O \rightarrow CH_2+HCO+H$). GRI21 and MRN98 do not exhibit significant positive SC's to C_2H_4 reactions. Interestingly, GRI30 has a noticeable positive SC to the vinyoxy-producing, $C_2H_3+O_2 \rightarrow CH_2CHO+O$.
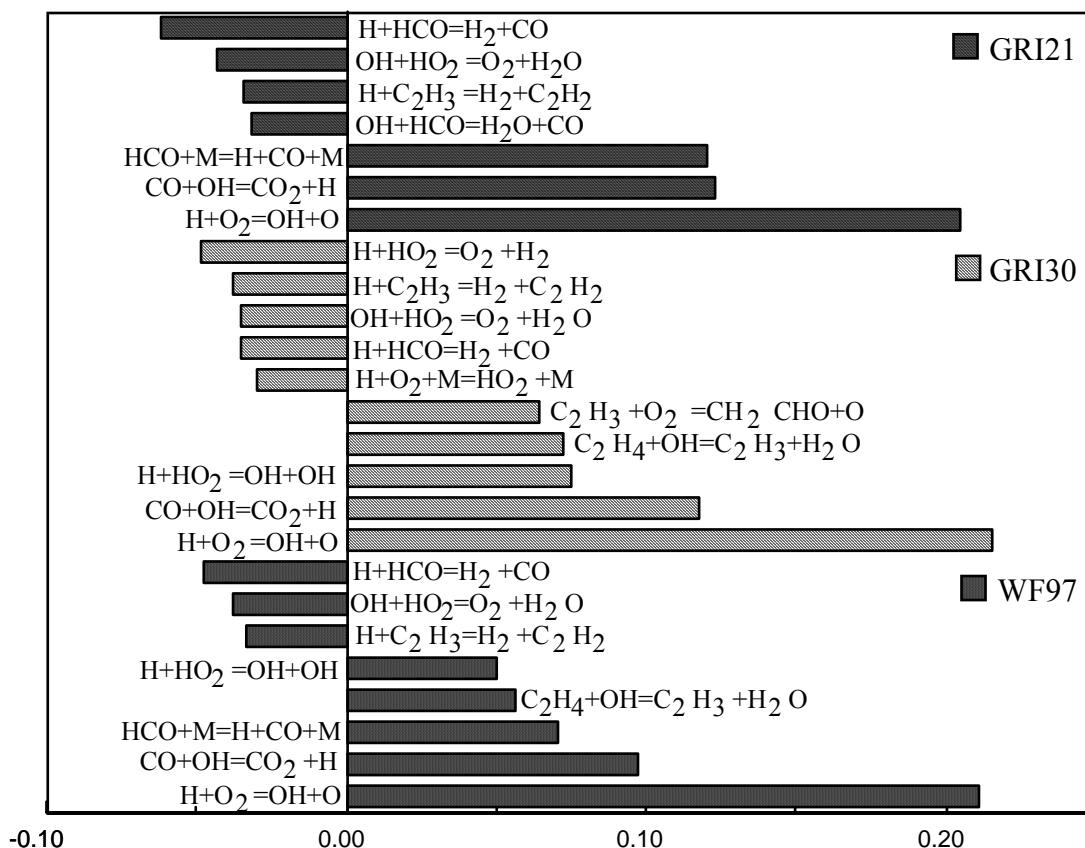
FIGURE 2. Normalized sensitivity coefficients on mass-burning rate for $\phi = 1.0$ C_2H_4/air flame: GRI21, GRI30, and WF97.

For all mechanisms considered, there is a noticeable negative SC to the H-terminating, $H+HCO \rightarrow H_2+CO$, as it competes for HCO with $HCO+M \rightarrow H+CO+M$. The three-body, $H+O_2+M \rightarrow HO_2+M$, has a significant terminating effect only for GRI30 and W99. GRI21, WF97, MRN98, and GRI30 exhibit negative SC's for $H+C_2H_3 \rightarrow H_2+C_2H_2$. Significant negative SC's to fuel reactions are exhibited only by TAN94. TAN94 also exhibits significant negative SC to $CH_3+CH_3 \rightarrow C_2H_5+H$.

While sensitivity analysis provides useful insights into rate-controlling mechanisms, it does not reveal the significance of kinetic steps that are not rate controlling, but may be important to the overall oxidation process. Thus, integrated-species consumption path analyses were performed for $\phi = 1.0$ flames. Table 1 contains the reactions referred to in the analysis below of flame propagation.

TABLE 1 Integrated percent species-consumption/-production analysis for one-dimensional, steady, planar, adiabatic, freely-propagating, laminar premixed flames, at $\phi = 1.0$.

C_2H_4-consumption		TAN94	GRI21	WF97	MRN98	GRI30	W99
R1	$C_2H_4+H \rightarrow C_2H_3+H_2$	13	30	28	31	26	12
R2	$C_2H_4+H+M \rightarrow C_2H_5+M$	16	8	10	9	7	6
R3	$C_2H_4+O \rightarrow CH_2CHO+H$	0	0	0	9	13	0
R4	$C_2H_4+O \rightarrow CH_3+HCO$	22	29	35	26	24	30
R5	$C_2H_4+O \rightarrow C_2H_3+OH$	0	0	0	0	0	14
R6	$C_2H_4+O \rightarrow C_2H^{(S)} + HCO+ H$	22	0	0	0	0	0
R7	$C_2H_4+OH \rightarrow C_2H_3+H_2O$	26	34	27	24	31	34
C_2H_3-consumption		TAN94	GRI21	WF97	MRN98	GRI30	W99
R8	$C_2H_3+H \rightarrow C_2H_2+H_2$	5	13	16	29	15	12
R9	$C_2H_3+O_2 \rightarrow HCO+CH_2O$	21	58	16	5	20	12
R10	$C_2H_3+O_2 \rightarrow C_2H_2+HO_2$	0	0	2	24	3	2
R11	$C_2H_3+O_2 \rightarrow CH_2CHO+O$	0	0	38	15	36	21
R12	$C_2H_3+M \rightarrow C_2H_2+H+M$	52	22	20	9	19	33
R13	$C_2H_3+CH_3+M \rightarrow C_3H_6+M$	16	0	0	0	0	0
CH$_2$CHO-consumption		TAN94	GRI21	WF97	MRN98	GRI30	W99
R14	$CH_2CHO+H \rightarrow CH_3+HCO$	0	0	0	20	8	41
R15	$CH_2CHO+O \rightarrow H+CH_2+CO_2$	0	0	0	0	12	0
R16	$CH_2CHO+O \rightarrow CH_2O+HCO$	0	0	0	12	0	0
R17	$CH_2CHO+OH \rightarrow HCO + CH_2OH$	0	0	0	0	9	0
R18	$CH_2CHO+OH \rightarrow CH_2CO + H_2O$	0	0	0	10	4	2
R19	$CH_2CHO+O_2 \rightarrow CH_2CO+HO_2$	0	0	0	0	0	12
R20	$CH_2CHO+M \rightarrow CH_2CO+H+M$	0	0	100	36	62	13
R21	$CH_2CHO+M \rightarrow CH_3+CO+M$	0	0	0	9	0	27
H-production		TAN94	GRI21	WF97	MRN98	GRI30	W99
R22	$H_2+OH \rightarrow H_2O+H$	16	17	17	17	17	13
R23	$H_2+O \rightarrow OH+H$	10	10	11	10	12	10
R24	$CO+OH \rightarrow CO_2+H$	36	41	36	33	38	42
R25	$HCO+M \rightarrow H+CO+M$	9	8	11	11	4	13

In the GRI21 mechanism, the fuel is consumed through reactions with H [R1(30%)], O [R4(29%)], and OH [R7(34%)]; the percentage indicates contribution of each reaction to the overall consumption. A minor contribution by the three-body Reaction R2(8%) is also noted. C_2H_3 is subsequently consumed through reactions with H [R8(13%)], O_2 [R9(58%)], and by the decomposition Reaction R12(22%). In the GRI30 mechanism, the fuel is consumed through Reactions H [R1(26%) and R2(7%)], O [R3(13%) and R4(24%)], and OH [R7(31%)]. C_2H_3 is subsequently consumed through reactions with H [R8(15%)], O_2 [R9(20%), R10(3%), and R11(36%)], and by the thermal decomposition Reaction R12(19%). CH_2CHO is consumed through reactions with the radicals H [R14(8%)], O [R15(12%)], OH [R17(9%) and R18(4%)], and through the thermal decomposition Reaction R20(62%).

There are significant differences between GRI21 and GRI30 at the fuel level. CH_2CHO is not included in GRI21, as previously noted (Egolfopoulos & Dimotakis 1998). GRI30 indicates production of CH_2CHO directly from the fuel (R3) and from C_2H_3 (R11). Subsequent reactions of CH_2CHO result in enhanced H-radical production, especially through R20. This partially explains the higher S_u^o values obtained in GRI30, compared to GRI21.

In the WF97 mechanism, the fuel is consumed through reactions with H [R1(28%) and R2(10%)], O [R4(35%)], and OH [R7(27%)]. C_2H_3 is subsequently consumed through reactions with H [R8(16%)], O_2 [R9(16%), R10(2%), and R11(38%)], and through the thermal decomposition Reaction R12(20%). CH_2CHO is entirely consumed through the thermal decomposition, $i.e.$, Reaction R20(100%). CH_2CHO is produced as in GRI30, yielding higher S_u^o's, compared to GRI21, since WF97 is an extension of GRI21, with the addition of CH_2CHO kinetics.

In the W99 mechanism, the fuel is consumed through reactions with H [R1(12%) and R2(6%)], O [R4(30%) and R5(14%)], and OH [R7(34%)]. C_2H_3 is subsequently consumed through reactions with H [R8(12%)], O_2 [R9(12%), R10(2%), and R11(21%)], and through the thermal decomposition Reaction R12(33%). CH_2CHO is consumed through reactions with H [R14(41%)], OH [R18(2%)], O2 [R19(12%)], and through the thermal decomposition Reactions R20(13%) and R21(27%).

W99 was optimized on experimental values for S_u^o (Egolfopoulos $et\ al.$ 1990) and, as a result, its values for S_u^o are closer to experiments, compared to the high GRI30 and WF97 values. While the latter two include CH_2CHO chemistry, W99 has a lower CH_2CHO H-

radical production rate (through R20), admitting additional consumption paths (R14 and R21), responsible for less-reactive products.
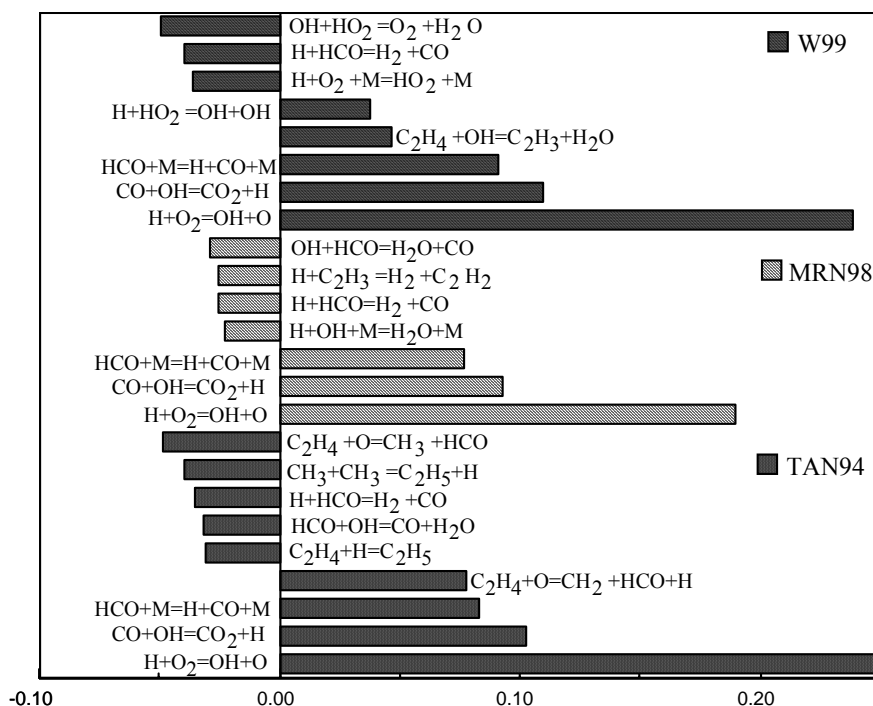

FIGURE 3. Normalized sensitivity coefficients on mass burning rate of $\phi = 1.0$ C_2H_4/air flame: W99, MRN98, and TAN94.

In MRN98, the fuel is consumed through reactions with H [R1(31%) and R2(9%)], O [R3(9%) and R4(26%)], and OH [R7(24%)]. C_2H_3 is subsequently consumed through reactions with H [R8(29%)], O_2 [R9(5%), R10(24%), and R11(15%)], and through the thermal-decomposition R12(19%). CH_2CHO is consumed through reactions with H [R14(20%)], O [R16(12%)], OH [R18(10%)], and through the thermal-decomposition Reactions R20(36%) and R21(9%). Note that among all mechanisms, only W99 and MRN98 allow for two decomposition channels. The relative importance between these two mechanisms appears to be different. More specifically, while in W99 R21 is twice as effective in decomposing CH_2CHO compared to R20, in MRN98 R21 is four times less effective compared to R20. This demonstrates the uncertainties associated with CH_2CHO chemistry in the various mechanisms. MRN98 is much slower than W99, even though it allows for the most efficient decomposition of CH_2CHO to CH_2CO and H, which enhances the overall oxidation process. The other kinetic subsets of MRN98 must, therefore, be substantially slower compared to W99.

Finally, in the TAN94 mechanism, the fuel is consumed through reactions with H [R1(13%) and R2(16%)], O [R4(22%) and R6(22%)] and OH [R7(26%)]. Note that R7, resulting in the singlet state $CH_2(S)$, is not considered in the fuel-consumption sequence by the other mechanisms considered. C_2H_3 is subsequently consumed through reactions with H [R8(5%)], O_2 [R9(21%)], through the thermal-decomposition R12(52%), and through the three-body recombination R13(16%). The contribution of R13 in C_2H_3 consumption is also unique among all mechanisms.

TAN94 does not include CH_2CHO, similarly to GRI21. At the same time, C_3 chemistry starts being important at the C_2H_3 consumption level through R13. This is not exhibited by the other mechanisms. Interestingly, W99 and TAN94, two significantly different mechanisms, calculate similar values of S_u^o. Of course, while failure to predict S_u^o is a deficiency, good prediction of S_u^o is only necessary.

Substantial differences between the mechanisms considered are apparent, not only in the contributions of the different reactions in consuming the parent fuel molecule, as well as important intermediates, but also in the steps that participate. Given the importance of H radicals in the overall response of the flame, the contributions of the various reactions to H-radical production were also studied. The results are also shown in Table 1. Reactions R22, R23, R24, and R25 involving H_2, CO, and HCO are chiefly responsible for the production of the H radicals, with contributions that are nearly mechanisms-independent. This reveals that all mechanisms agree closely at the H_2/CO/HCO level; kinetics that are best understood among all species relevant to combustion.

4.3 Ignition/extinction response of non-premixed flames

Figure 4 compares the Z-curve response for all six mechanisms. The turning point at the largest value of σ represents the extinction strain rate, σ_{ext}. The turning point at the lowest value represents the ignition strain rate, σ_{ign}.

Results in Fig. 4 reveal Z-curves that differ not only in the values of σ_{ign} and σ_{ext}, but also in shape. Notably, while GRI30 is a derivative of GRI21, with CH_2CHO chemistry added, the corresponding predicted Z-curves are significantly different. The two GRI mechanisms bound the predictions of the six mechanisms. Also, while MRN98 and TAN94 (marginally)

exhibit two-stage ignition behavior, the other mechanisms do not, although they have a noticeable change in slope at larger Y_{Hmax} values. Since higher Y_{Hmax} implies higher prevailing temperatures in the reaction zone, one can expect differences between these mechanisms over a wide range of temperatures.
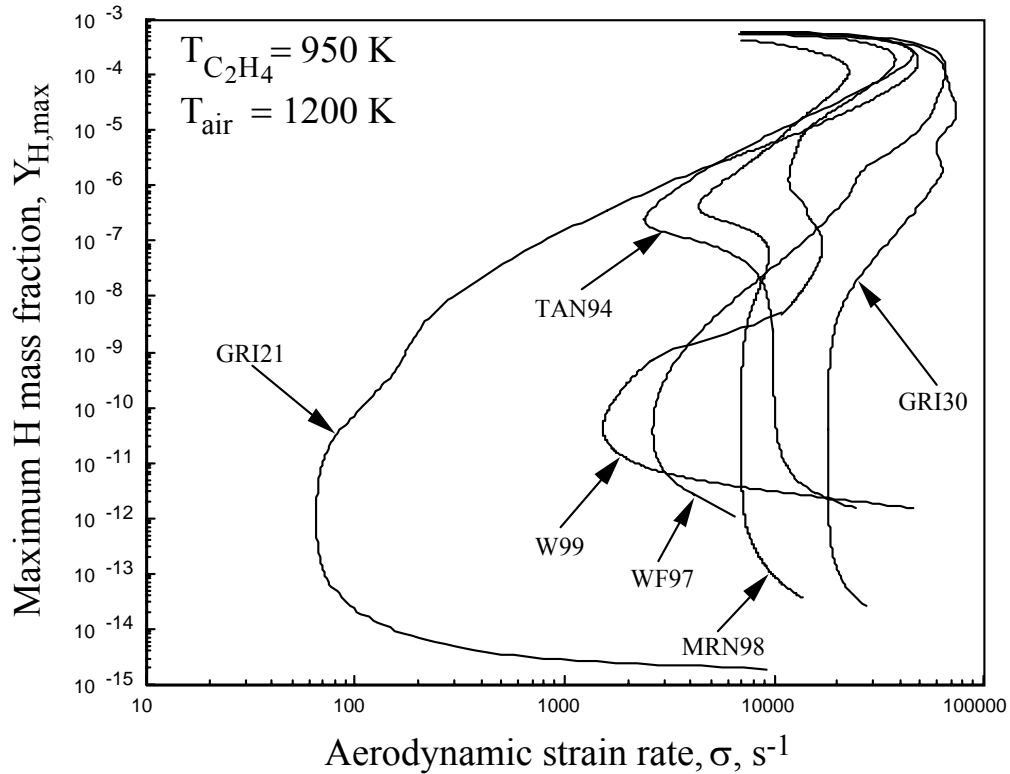

FIGURE 4. Calculated Z-curve response of non-premixed C_2H_4/air (T_{air} = 1200 K, T_{fuel} = 950 K).

Figure 5 depicts the values of σ_{ign} and σ_{ext} calculated by all mechanisms, scaled by GRI21 values. Figure 5a depicts σ_{ign} results. They differ by factors as high as 300. Figure 5b depicts results for σ_{ext}, as well as for S_u^o, for both stoichiometric and rich flames. S_u^o values were included because flame propagation and extinction are high-temperature phenomena controlled by similar kinetics. Figure 5b illustrates this point, with larger S_u^o values corresponding to larger σ_{ext}'s. The differences in the two quantities can be understood by the fact that convective transport and attendant flame-temperature-reduction influence extinction, effects that do not enter in one-dimensional, freely propagating flame models.
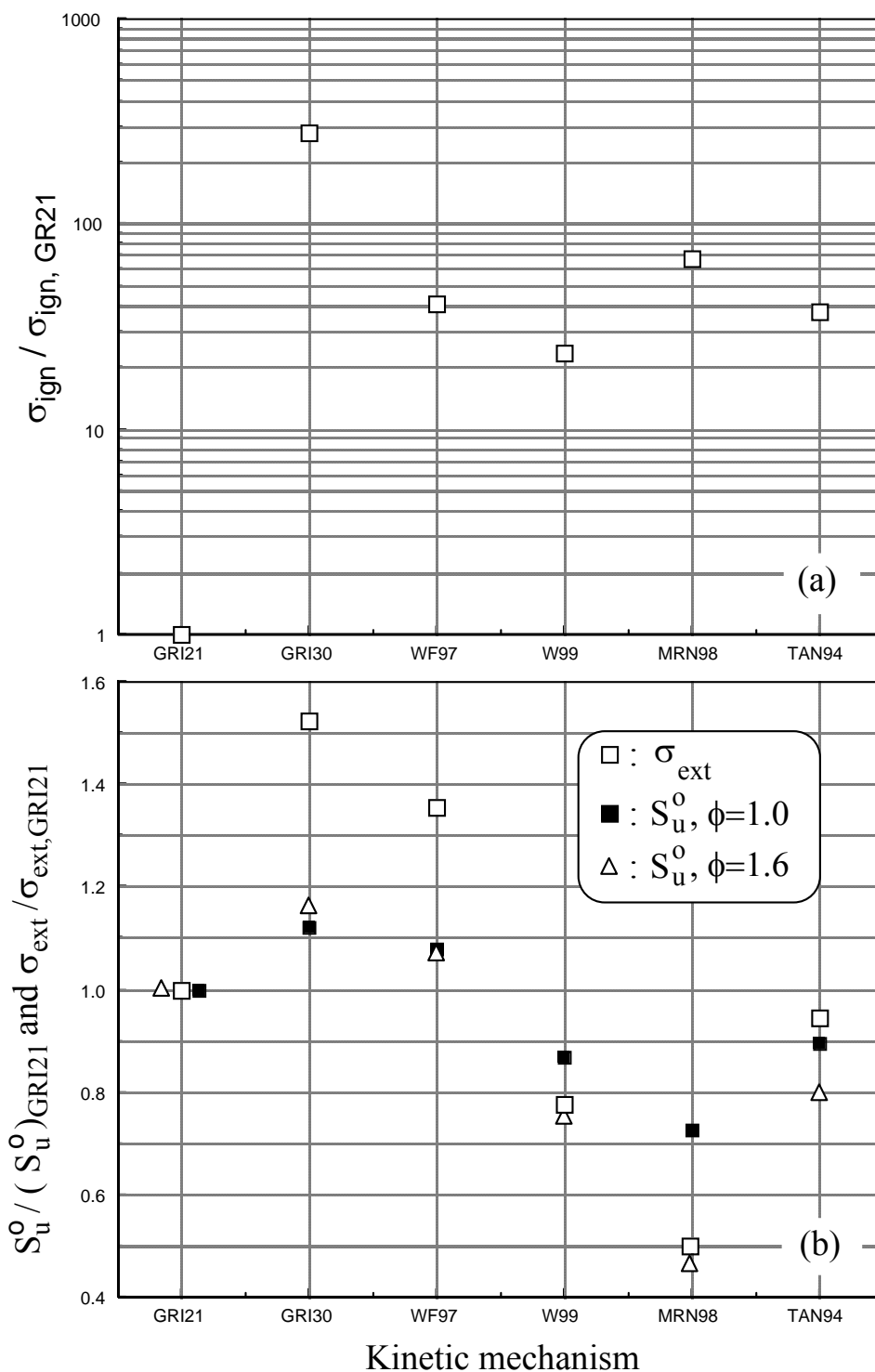
FIGURE 5. Calculated ignition and extinction strain rates (5a) for non-premixed C_2H_4/air for T_{air} = 1200 K and T_{fuel} = 950 K, and laminar flame speeds (5b) for ϕ = 1.0 and ϕ = 1.6 C_2H_4/air flames, scaled by the corresponding GRI21 values.

Low-temperature kinetics were assessed at the ignition points of all Z-curves (Fig. 4). For the MRN98 and TAN94 Z-curves, that exhibit two-stage ignition behavior, the lower-ignition point was taken at Y_{Hmax} values in the range of 10^{-11} to 10^{-10}. In all cases, integrated species-consumption analysis was conducted. The contributions of the most important reactions are listed in Table 2. In this regime, the fuel is consumed in GRI21 through reactions with O [R4(7%)], OH [R7(10%)], HO_2 [R27(12%)], and the thermal-decomposition R26(59%). C_2H_3 is entirely decomposed through R9(100%). H radicals that are important for ignition are produced through the thermal-decomposition reactions, R25(15%), R31(74%), and R34(2%).

In GRI30, the fuel is consumed through reactions with H [R2(13%)], O [R3(12%) and R4(22%)], OH [R27(20%)], CH_3 [R29(7%)], and the thermal-decomposition R26(20%). C_2H_3 is subsequently consumed through reactions with O_2 [R9(40%) and R11(56%)]. CH_3, produced in significant amounts by R4, is consumed through reaction with C_2H_4 [R29(89%)]. Thus, C_2H_3 is the main product of fuel consumption.

CH_2CHO is consumed through reactions with O_2 [R30(6%)] and the thermal-decomposition R20(87%). H radicals are produced through R3(30%), R20(65%), R25(5%), and R34(1%). Apparently, the contribution of the thermal-decomposition reactions to H production is reduced compared to the GRI21. Comparing GRI21 and GRI30, it is apparent that CH_2CHO chemistry in GRI30 results in more efficient H-radical production, favoring ignition.

In the WF97 mechanism, the fuel is consumed through reactions with H [R2(13%)], O [R4(39%)], OH [R7(18%)], CH_3 [R29(21%)], and the thermal-decomposition R26(2%). C_2H_3 is consumed by O_2 [R9(37%) and R11(58%)], as in GRI30. CH_2CHO is entirely decomposed through R20(100%) to CH_2CO and H; R20 is mostly (83%) responsible for H-radical production. Additional contributions to H-production are realized by R25(14%) and R36(3%).

In the W99 mechanism, the fuel is consumed through reactions with H [R2(4%)], O [R4(30%) and R5(9%)], OH [R7(27%)], CH_3 [R29(21%)], and to a minor extent by the thermal-decomposition R26(1%). C_2H_3 is consumed by O_2 [R9(36%) and R11(60%)], as in WF97 and GRI30. CH_2CHO is consumed through reactions with O_2 [R19(66%) and R30(9%)], and the thermal-decomposition R20(6%) and R21(19%). H radicals are produced through the thermal-decomposition reactions, R20(18%), R25(43%), and R34(12%), as well

as R33(20%). CH_2CHO is of lower importance in direct H-radical production, with lower σ_{ign} compared to both WF97 and GRI30.

TABLE 2 Integrated percent species-consumption/-production analysis, at lower-ignition point, of strained laminar C_2H_4/air non-premixed flames.

C_2H_4-consumption		TAN94	GRI21	WF97	MRN98	GRI30	W99
R2	$C_2H_4+H+M \rightarrow C_2H_5+M$	7	0	13	11	13	4
R3	$C_2H_4+O \rightarrow CH_2CHO+H$	0	0	0	8	12	0
R4	$C_2H_4+O \rightarrow CH_3+HCO$	13	7	39	24	22	30
R5	$C_2H_4+O \rightarrow C_2H_3+OH$	0	0	0	0	0	9
R6	$C_2H_4+O \rightarrow C_2H^{(S)} + HCO+ H$	13	0	0	0	0	0
R7	$C_2H_4+OH \rightarrow C_2H_3+H_2O$	37	10	18	18	20	27
R26	$C_2H_4+M \rightarrow H_2+C_2H_2+M$	1	59	2	11	20	1
R27	$C_2H_4+HO_2 \rightarrow C_2H_5+O_2$	0	12	0	0	0	0
R28	$C_2H_4+HO_2 \rightarrow C_2H_4O+OH$	15	0	0	0	0	0
R29	$C_2H_4+CH_3 \rightarrow C_2H_3+CH_4$	10	5	21	20	7	21
C_2H_3-consumption		TAN94	GRI21	WF97	MRN98	GRI30	W99
R9	$C_2H_3+O_2 \rightarrow HCO+CH_2O$	100	100	37	41	40	36
R11	$C_2H_3+O_2 \rightarrow CH_2CHO+O$	0	0	58	57	56	60
CH_2CHO-consumption		TAN94	GRI21	WF97	MRN98	GRI30	W99
R19	$CH_2CHO+O_2 \rightarrow CH_2CO+HO_2$	0	0	0	0	0	66
R30	$CH_2CHO+O_2 \rightarrow CH_2O+CO+OH$	0	0	0	28	6	9
R20	$CH_2CHO+M \rightarrow CH_2CO+H+M$	0	0	100	53	87	6
R21	$CH_2CHO+M \rightarrow CH_3+CO+M$	0	0	0	19	0	19
H-production		TAN94	GRI21	WF97	MRN98	GRI30	W99
R3	$C_2H_4+O \rightarrow CH_2CHO+H$	0	0	0	29	30	0
R6	$C_2H_4+O \rightarrow CH_2^{(S)}+HCO+H$	43	0	0	0	0	0
R20	$CH_2CHO+M \rightarrow CH_2CO+H+M$	0	0	83	56	65	18
R25	$HCO+M \rightarrow CO+H+M$	28	15	14	11	5	43
R31	$C_2H_5+M \rightarrow H+C_2H_4+M$	0	74	0	0	0	0
R32	$CH_2+O_2 \rightarrow CO_2+H+H$	16	0	0	0	0	0
R33	$C_2H_4+CH_3 \rightarrow C_3H_6+H$	0	0	0	0	0	20
R34	$CH_3O+M \rightarrow CH_2O+H+M$	1	2	3	1	1	12

In MRN98, the fuel is consumed through reactions with H [R2(11%)], O [R3(8%) and R4(24%)], OH [R7(18%)], CH_3 [R29(20%)], and by the thermal-decomposition R26(11%). As in WF97, GRI30, and W99, C_2H_3 reacts with O_2 [R9(41%) and R11(57%)] to produce CH_2O/HCO and CH_2CHO. CH_2CHO is consumed through reaction with O_2 [R30(28%)] and through the thermal-decomposition R20(53%) and R21(19%). H radicals are produced through the thermal-decomposition R20(56%), R25(11%), and R34(1%), as well as R3(29%). MRN98 and GRI30 are similar, with CH_2CHO produced directly from the fuel and H-radicals produced via CH_2CHO decomposition to H and CH_2CO.

In TAN94, the fuel is consumed through reactions with H [R2(7%)], O [R4(13%) and R6(13%)], OH [R7(37%)], HO_2 [R28(15%)], CH_3 [R29(10%)], and by the thermal-decomposition R26(1%). Given the omission of CH_2CHO chemistry, C_2H_3 is entirely consumed by O_2 [R9(100%)] to form CH_2O and HCO, with C_2H_4O readily decomposing to CH_3 and HCO. H radicals are produced through R6(43%) and R32(16%), and through the thermal-decomposition R25(28%) and R34(1%). TAN94 is unique compared to the other mechanisms; it omits CH_2CHO and introduces C_2H_4O as a product of fuel oxidation.

Comparing the details of all mechanisms at the ignition point, significant differences can be seen at all oxidation levels. For example, the fuel consumption paths vary noticeably, which in turn affects the production rate of C_2H_3. The most profound difference between all mechanisms, however, is the kinetics of CH_2CHO, which are either missing, *e.g.*, TAN94 and GRI21, or are characterized by very different steps and rates by the various mechanisms. As shown in Table 2, this has a direct consequence on H-radical production, which varies significantly between the mechanisms considered.

In summary and as can be seen in Tables 1 and 2, dominant species and reactions responsible for H-radical production vary significantly between propagation and extinction, on the one hand, and ignition on the other. This difference is explained by the fact that propagation and extinction entail high-activation-energy kinetics of small molecules, *e.g.*, H_2, CO, and HCO, which are fast at the high temperatures that control flame propagation and extinction. In contrast, ignition entails lower-activation-energy kinetics of large molecules, compositionally close to the parent fuel, which dominate kinetically at the lower temperatures relevant to ignition. The closer agreement between predictions of propagation and extinction between mechanisms can be traced to the better understanding and agreement

of the kinetics of the smaller species. The large variance between ignition predictions is a manifestation of the significant uncertainties in the kinetics of larger species.

5. CONCLUDING REMARKS

A comparative study of six available mechanisms that include C_2H_4 kinetics was conducted in flames. Laminar-flame propagation for C_2H_4/air mixtures and ignition/extinction (Z-curves) of non-premixed, counterflowing C_2H_4 and air were simulated. Non-premixed extinction/ignition response was determined for conditions of relevance to SCRAMJET concepts involving endothermic hydrocarbons, where C_2H_4 will be an important constituent of thermally cracked fuel.

Comparisons for both premixed and non-premixed flames reveal large differences between the mechanisms in predicted laminar flame speeds, as well as in ignition/extinction strain rates. Variations as high as a factor of 2.5 for laminar flame speeds, factors of 3 for extinction, and factors in the range 100-300 for ignition strain rates were found.

Analysis of flame structure reveals significant differences between the mechanisms at the C_2H_3 oxidation level. In particular, while some mechanisms include CH_2CHO, others do not. CH_2CHO is important in the production of H radicals, on which flame speed has a dominant dependence, and which increase both ignition and extinction strain rates. Unfortunately, there are large uncertainties in CH_2CHO kinetics. The role of C_3 chemistry is also not clear, contributing in some mechanisms, but not in all.

Comparisons with available experimental laminar flame-speed data proved useful. The dimensionality of the unknowns in the kinetic mechanisms, is very high, and will require a suite of experiments to provide additional validation data, including ignition and extinction, under variable-pressure conditions. These are required only for C_2H_4 but also for other hydrocarbons and hydrocarbon blends whose kinetics are described by the same mechanisms. At this time, limited experimental data are available for only some small hydrocarbons, mostly at one atmosphere, and do not readily facilitate validation of the relative importance of two- and three-body reactions, for example.

Acknowledgments

References

Bhargava, A. & Westmoreland, P.R. 1998a Measured Flame Structure and Kinetics in a Fuel-Rich Ethylene Flame. *Combust. Flame* 113: 333-347

Bhargava, A. & Westmoreland, P.R. 1998b MBMS Analysis of a Fuel-Lean Ethylene Flame. *Combust. Flame* 115: 456-467.

Bowman, C.T., Frenklach, M., Gardiner, W.R. & Smith, G. 1999 "The 'GRI 3.0' Chemical Kinetic Mechanism." http://www.me.berkeley.edu/gri_mech/.

Davis, S.G., Law, C.K. & Wang, H. 1999 Propene Pyrolysis and Oxidation Kinetics in Flow Reactor and Laminar Flames. *Combust. Flame* 119: 375-399.

Edwards, T. 1996 Fuels and Fuel System Area: Air Force Perspective. AFOSR/NASA Workshop on Supersonic Scramjet Combustion, 13-16 May 1996, Newport News, VA.

Egolfopoulos, F.N. 1994 Dynamics and Structure of Unsteady, Strained, Laminar, Premixed Flames. *Proc. Combust. Inst.* 25: 1365-1373.

Egolfopoulos, F.N. & Campbell C.S. 1996 Unsteady, Counterflowing, Strained Diffusion Flames: Frequency Response and Scaling. *J. Fluid Mech.*, 318: 1-29.

Egolfopoulos, F.N. & Dimotakis, P.E. 1998 Non-Premixed Hydrocarbon Ignition at High Strain Rates. *Proc. Combust. Inst.* 27: 641-648.

Egolfopoulos, F.N. & Dimotakis, P.E. 2000 Effects of Additives on the Non-Premixed Ignition of Ethylene in Air. *Combust. Sci. Tech.* 156: 173-199.

Egolfopoulos, F.N., Zhu, D.L. & Law, C.K. 1990   Experimental and Numerical Determination of Laminar Flame Speeds: Mixtures of C_2-Hydrocarbons with Oxygen and Nitrogen. *Proc. Combust. Inst.* 23: 471-478.

Frenklach, M., Wang, H., Goldenberg, M., Smith, G.P., Golden, D.M., Bowman, C.T., Hanson, R.K., Gardiner, W.C. & Lissianski, V. 1995   GRI-Mech–An Optimized Detailed Chemical Reaction Mechanism for Methane Combustion.   GRI Technical Report No. GRI-95/0058.

Kee, R. J., Warnatz, J. & Miller J.A. 1983   A FORTRAN Computer Code Package for the Evaluation of Gas-Phase Viscosities, Conductivities, and Diffusion Coefficients.   Sandia Report SAND83-8209.

Kee, R.J., Grcar, J. F., Smooke, M.D. & Miller J.A. 1985   A FORTRAN Program for Modeling Steady Laminar One-Dimensional Premixed Flames.   Sandia Report SAND85-8240.

Kee, R. J., Rupley, F. M. & Miller J.A. 1989 Chemkin-II: A FORTRAN Chemical Kinetics Package for the Analysis of Gas-Phase Chemical Kinetics. Sandia Report SAND89-8009.

Laskin, A. & Wang, H. 1999 On initiation reactions of acetylene oxidation in shock tubes. *Chem. Phys. Lett*. 303, 43-49.

Law, C.K. & Egolfopoulos, F.N. 1992   A Unified Chain-Thermal Theory of Fundamental Flammability Limits. *Proc. Combust. Inst.* 24: 137-144.

Marinov, N.M. (1998) "A Detailed Chemical Kinetic Model for High Temperature Ethanol Oxidation," *Int. J. Chem. Kin*., in press.

Marinov, N.M., Pitz, W.J. & Westbrook, C.K. 1995   Numerical Study of Ethylene and Acetylene Laminar Flame Speeds.   Joint Technical Meeting, Central States and Western States Section/CI, April 23-26.

Nishioka, M., Law, C.K. & Takeno, T. 1996 A Flame-Controlling Continuation Method for Generating S-Curve Responses with Detailed Chemistry.   *Combust. Flame* 104: 328-342.

Sun, C.J., Sung, C.J., Wang, H. & Law, C.K. 1996 On the Structure of Non-Sooting Counterflow Ethylene and Acetylene Diffusion Flames. *Combust. Flame* 107, 321-335.

Tan, Y., Dagaut, P., Cathonnet, M., Boettner, J.C., Bachman, J.S. & Carlier, P. 1994 Natural Gas and Blends Oxidation and Ignition: Experiments and Modeling. *Proc. Combust. Inst.* 25: 1563-1569.

Wang, H. & Frenklach, M. 1997 A Detailed Kinetic Modeling Study of Aromatics Formation in Laminar Premixed Acetylene and Ethylene Flames. *Combust. and Flame* 110:173-221.

Wang, H., Laskin, A., Djurisic, Z. M., Law, C. K., Davis, S. G. & Zhu, D. L. 1999 A comprehensive mechanism of C_2H_x and C_3H_x fuel combustion. Chemical and Physical Processes of Combustion, the 1999 Fall Technical Meeting of the Eastern States Section of the Combustion Institute, Raleigh, NC, pp. 129-132.

Westbrook, C.K. & Dryer, F.L. 1981 Chemical Kinetics and Modeling of Combustion Processes. *Proc. Combust. Inst.* 18: 749-767.